ELSEVIER

Polymer 44 (2003) 2965–2974

polymer

www.elsevier.com/locate/polymer

Comparison of hydrogen bonding interaction between PMMA/PMAA blends and PMMA-*co*-PMAA copolymers

Chih-Feng Huang, Feng-Chih Chang*

Institute of Applied Chemistry, National Chiao Tung University, 1001 Ta Hsuen Road, Hsin Chu 30050, Taiwan, ROC

Received 10 September 2002; received in revised form 25 November 2002; accepted 21 February 2003

Abstract

A series of miscible PMMA/PMAA blends and PMMA-*co*-PMAA copolymers with different compositions were prepared in this study. T_gs of PMMA-*co*-PMAA copolymers are significantly higher than average values or from the Fox equation. The proton spin-lattice relaxation time in the rotating frame ($T_{1\rho}^H$) determined by high resolution solid state ^{13}C nuclear magnetic resonance indicates single composition-dependent from all blends and copolymers, implying a good miscibility with chain dynamics on a scale of 1–2 nm. However, $T_{1\rho}^H$s of copolymers are still smaller than those of blends, implying that degrees of homogeneity of copolymers are higher than those of blends. On the basis of Kovacs' free volume theory, the free volume of the copolymer obtained is decreased which is another indication of greater homogeneity of the copolymer than that of the corresponding blend. According to Fourier transform infrared spectroscopy analyses, the above results can be rationalized that the hydrogen bonding interaction of the copolymer is stronger than the blend.

Keywords: Hydrogen bond; Blends; Copolymers

1. Introduction

Polymers possessing high glass transition temperature provide attractive interest in polymer science due to strong economic incentives arising from their special applications. For example, the glass transition temperature of poly(methyl methacrylate) (PMMA) is about 100 °C that tends to limit its applications in optical-electronic industry such as compact disk (CD), optical glass and optical fiber. Polycarbonate has been widely used in optical devices due to its high transparency and high glass transition temperature (ca. 150 °C). However, polycarbonate has absorption at blue light laser (ca. 400 nm) preventing its application in the new high-density digital versatile disk (HD-DVD) (15 GB). Recently, the cyclo olefin copolymer (COC) [1–3] has the potential to replace polycarbonate for HD-DVD due to its high transparency at blue light laser and high glass transition temperature. PMMA has the chance to replace polycarbonate for HD-DVD application due to its high transparency at blue light laser and lower cost. Nevertheless, the PMMA has to be modified to raise its glass transition temperature. By blending the PMMA with polymers containing rigid or bulky structure is considered as an easy way to achieve higher glass transition temperature, however, problem of immiscibility with phase separation is usually encountered. Recently, copolymerization of methyl methacrylate with rigid or bulky monomer, such as maleic anhydride, cyclohexyl methylacrylate or methacrylmethyl-methylimides, has been reported to overcome the immiscibility and phase separation problems. However, the predicted glass transition temperature generally obeys or lower than that from the Fox rule, the increase in glass transition temperature is limited unless higher content of the rigid monomer is employed.

In our previous study [4], we have found that the glass transition temperature of the miscible blend of poly(vinylphenol) (PVPh) and poly(vinylpyrrolidone) is significantly higher than the corresponding value predicted by the Fox rule [1], indicating that this blend system must involve certain specific interaction. Furthermore, Coleman et al. [5] reported that the glass transition temperature of poly(vinylphenol-*co*-ethyl methacrylate) is higher than the polymer blend with identical composition due to relatively stronger hydrogen bonding of the copolymer. According to the Painter–Coleman association model [6], the inter-association

* Corresponding author. Tel.: +886-3-5727077; fax: +886-3-5719507.
E-mail address: changfc@cc.nctu.edu.tw (F.C. Chang).

0032-3861/03/$ - see front matter © 2003 Elsevier Science Ltd. All rights reserved.
doi:10.1016/S0032-3861(03)00188-5

equilibrium constant of hydrogen bonding in poly(vinylphenol-*co*-ethyl methacrylate) ($K_A = 67.4$) is higher than that of the inter-association equilibrium constant of the poly(vinylphenol)/poly(ethyl methacrylate) blend ($K_A = 37.4$), implying that T_g for the copolymer and blend of the same composition should be different. In other words, the nature of hydrogen bonding in a blend and its copolymer must be different.

In this study, poly(MMA-*co*-MAA) with different monomer ratios were prepared by free radical copolymerization in toluene. Characterizations were carried out by gel permeation chromatography (GPC), differential scanning calorimetry (DSC), Fourier transform infrared spectroscopy (FT-IR), and high-resolution solid-state ^{13}C nuclear magnetic resonance (NMR) spectroscopy.

2. Experimental

2.1. Materials

Methyl methacrylate (MMA, Aldrich) was destabilized, vacuum-distilled, and stored under nitrogen below 0 °C. The reagent grade methacrylic acid (MAA, Aldrich) was distilled under reduced pressure prior to use. 2,2′-azobisisobutyronitrile (AIBN, Acros) was recrystallized from acetone. *N*,*N*′-dimethylformamide (DMF), cyclohexane, and toluene were distilled, respectively, from magnesium sulfate and sodium/benzophenone immediately before use.

2.2. Blend preparation

Desired composition of PMMA and PMAA was dissolved in DMF at a concentration of 5 wt% and stirred for 6–8 h. The solution was allowed to evaporate slowly at 50 °C for 1 day on a Teflon plate and dried at 90 °C for 3 days to ensure total elimination of the solvent.

2.3. Preparation and characterization of homopolymers and copolymers

The homopolymer and copolymer samples were prepared by 80 °C in toluene (75 vol%) under nitrogen using AIBN (0.015 mol l^{-1}) as initiator. The reaction mixture was dissolved in toluene and poured into cyclohexane after 24 h. A series of copolymers were prepared having different MMA and MAA monomer concentrations. MAA contents, molecular masses (M_w) and conversion are summarized in Table 1. The molar mass was determined at 85 °C by GPC from WATERS equipped with four μ-styragel columns using DMF as the solvent. The chemical composition of the copolymer was measured by titration in methanol/tetrahydrofuran co-solvent.

The reactivity ratio of copolymerization was determined by employing the Kelen–Tudos method [7]. This method derives the reactivity ratio from the well-known 'copolymerization equation' which contains two parameters, η and ξ, as described in our previous study [8]. Fig. 1 shows the Kelen–Tudos plot for PMMA-*co*-PMAA copolymers. By interpolating the experimental values (η as a function of ξ), we can obtain the reactivity ratios for methyl methacrylate $r_{MMA} = 0.25$ and for methacrylic acid $r_{MAA} = 0.72$. The sequence distribution of copolymers were predicted using the reactivity ratios based on the statistical relations that both copolymerization systems resulted in a predominantly random distribution of the monomeric units in the copolymer chain [9,10]:

$$P_{12} = 1 - P_{11} = \frac{1}{1 + r_1 X}$$

$$P_{21} = 1 - P_{22} = \frac{1}{1 + r_2/X}$$

where P_{ij} $(i, j = 1, 2)$ are the conditional probabilities of the addition of monomer j to a growing chain ending in an active i radical and the $X = [M_1]/[M_2]$ is the composition of the monomer feed. M_1 and M_2 represent MMA and MAA monomers, respectively. The probabilities for the first-order Markovian model of copolymerization, P_{12} and P_{21} are summarized in Table 1.

Table 1
Characteristics of homopolymers and copolymers

F_1 (feed)	f_1 (copolymer)	M_n (g/mol)	M_w (g/mol)	M_w/M_n	P_{12}	P_{21}
0.00	0.00	15 900	44 200	2.78	0.000	0.000
0.09	0.10	17 100	45 300	2.65	0.976	0.121
0.27	0.30	16 500	42 900	2.60	0.915	0.339
0.47	0.41	16 700	44 400	2.66	0.818	0.552
0.67	0.54	17 100	45 000	2.63	0.663	0.738
0.88	0.71	17 800	44 300	2.49	0.353	0.911
1.00	1.00	18 300	43 700	2.39	0.000	0.000

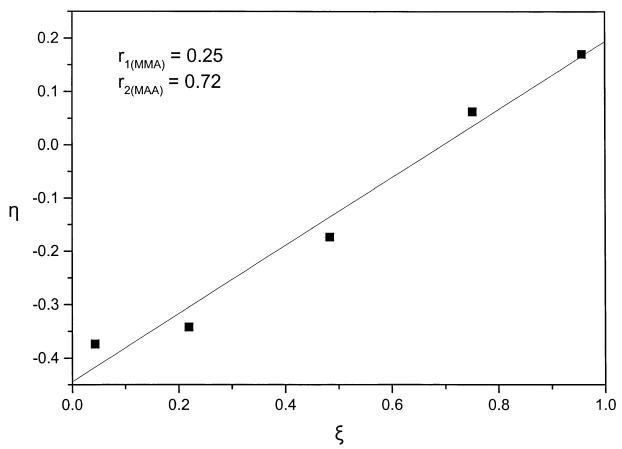

Fig. 1. Kelen–Tudos plot for PMMA-*co*-PMAA copolymers.

2.4. Differential scanning calorimetry (DSC)

Thermal analysis was carried out on a DSC instrument from DuPont (model 910 DSC-9000 controller) with a scan rate of 20 °C/min and a temperature range of 30–170 °C in nitrogen atmosphere and isothermal for 5 min to evaporate solvent. Approximately 5–10 mg sample was weighed and sealed in an aluminum pan. The sample was quickly cooled to room temperature from the first scan and then scanned between 30 and 280 °C at a scan rate of 20 °C/min. The glass transition temperature is taken as the midpoint of the heat capacity transition between the upper and lower points of deviation from the extrapolated glass and liquid lines.

2.5. FT-IR spectra

FT-IR measurement was made using a Nicolet Avatar 320 FT-IR spectrometer, 32 scans at a resolution of 1 cm^{-1} were collected with a NaCl disk. The DMF solution containing the sample was cast onto a NaCl disk and dried under condition similar to that used in bulk preparation. The sample chamber was purged with nitrogen in order to maintain the film dryness.

2.6. Solid-state NMR

High-resolution solid-state ^{13}C NMR experiments were carried out at room temperature using a Bruker DSX-400 spectrometer operating at a resonance frequency of 100.47 MHz for ^{13}C. The high-resolution solid-state ^{13}C NMR spectra were acquired by using the cross-polarization (CP)/magic angle spinning (MAS)/high-power dipolar decoupling technique. A 90° pulse width of 3.9 μs with 3 s pulse delay time and an acquisition time of 30 ms with 2048 scans were used. A magic angle sample-spinning rate of 5.4 KHz was used to avoid absorption overlapping. The proton spin-lattice relaxation time in the rotating frame ($T_{1\rho}^{H}$) was determined indirectly via carbon observation using a 90°–τ–spin lock pulse sequence prior to CP. The data acquisition was performed at a delay time (τ) ranging from 0.1 to 12 ms with a contact time of 1.0 ms.

2.7. Excess volume measurement

The specific volume was determined at 298.15 K using a pycnometer calibrated with *n*-heptane. The excess volume is define as follow:

$$V_e = V - (w_a V_a^0 + w_b V_b^0) \quad (1)$$

where w_i is the weight fraction of i component, V_i^0 is the specific volume of the ith pure component, and V is the specific volume of the sample.

3. Results and discussion

3.1. DSC and FT-IR spectra analyses

In general, the DSC analysis is one of the most convenient methods to determine the miscibility in polymer blends. The glass transition temperatures of these pure polymers synthesized in this study, PMMA and PMAA, are 104 and 170 °C, respectively. Fig. 2 shows the conventional second run DSC thermograms of these homopolymers and PMMA/PMAA blends with various weight ratios (80/20, 60/40, 40/60, 20/80). Essentially, all these PMMA/PMAA blends have a single T_g. There is an endothermic peak in all blends as shown in Figs. 2 and 3 and we will discuss this phenomenon later. A single T_g strongly suggests that these blends are fully miscible with a dimension on the order of 20–40 nm. Essentially, all T_gs are below the liner relationship of mother polymers. Generally, if T_g-composition relationship is negative deviation, neither a linear relationship nor the ideal rule of Fox is applicable [11]. The Fox equation describes the T_g relationship for most polymer mixtures with good molecular-scale mixing without aggregation or specific interaction. To quantitative assess the degree of interactions between PMMA and PMAA segments, the Kwei equation is the most popular equation to predict the variation of glass transition temperature [12] by

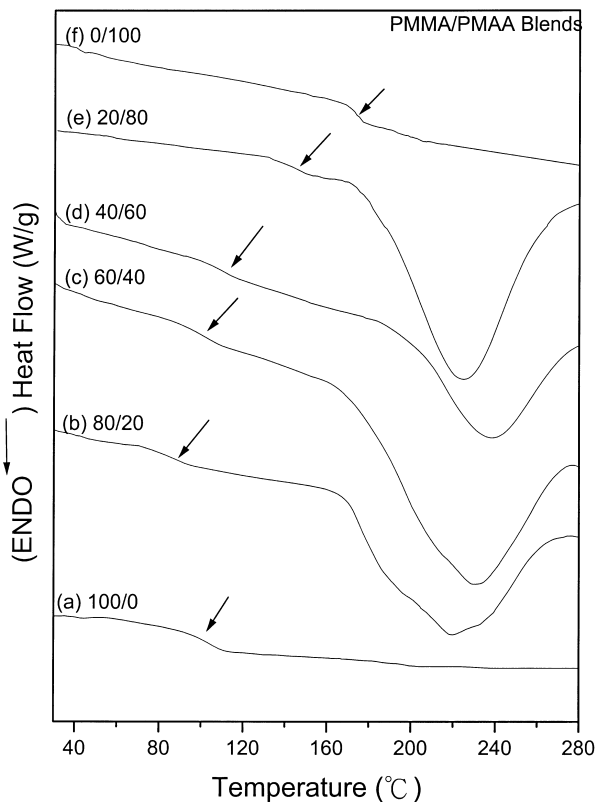

Fig. 2. DSC thermograms of the PMMA/PMAA blends with different compositions (weight ratio): (a) 100/0 (b) 80/20 (c) 60/40 (d) 20/80 (e) 0/100.

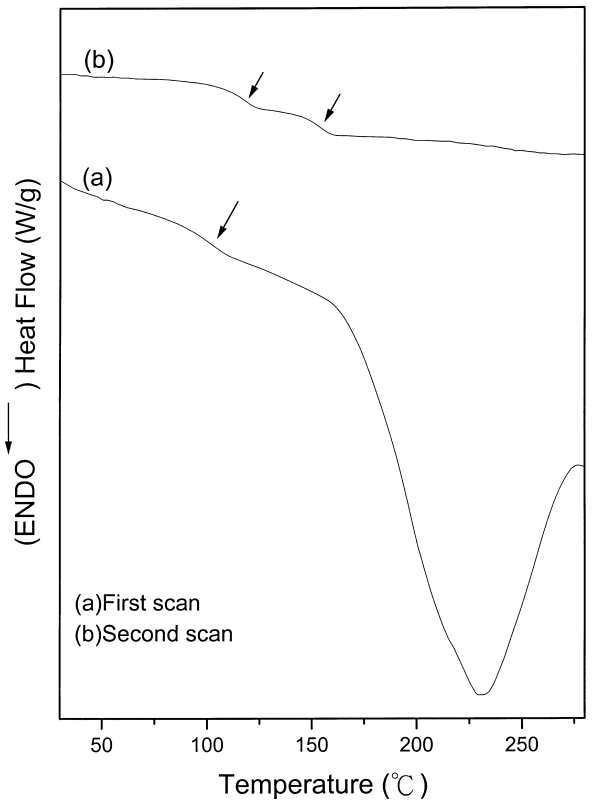

Fig. 3. DSC thermograms of the 60PMMA/40PMAA blend: (a) single T_g before phase separation and the endothermic peak of phase separation (b) second run after phase separation.

the following T_g-composition relationship:

$$T_g = \frac{W_1 T_{g1} + kW_2 T_{g2}}{W_1 + kW_2} + qW_1 W_2 \quad (2)$$

where W_1 and W_2 are weight fractions of compositions, T_{g1} and T_{g2} represent the corresponding glass transition temperatures, k and q are fitting constants. As shown in Fig. 4 curve (d), $k = 1$ and $q = -133$ are obtained from the non-linear least-squares 'best fit' values [13]. The q is a parameter corresponding to the strength of hydrogen bonding in the blend, reflecting a balance between the breaking of the self-association and the forming of the inter-association hydrogen bonding. A negative q of -133 implies that the self-association interaction is stronger than the inter-association interaction between PMMA and PMAA, resulting in free volume increase. Iriate et al. [14] have proposed that the effect of the free volume term for weaker hydrogen bonding plays an important role. We will go on for further discussion later on the free volume term contribution. Notably, there is a phase-separation associated with an endothermic process in all blends as shown in Fig. 2. According to prior literature [15–17], the phase separation at higher temperature of these PMMA/PMAA blends can be attributed to the lower critical solution temperature phenomenon. Positive and negative values have been reported for different blends. The position and area of the endothermic peak depends on the interaction strength

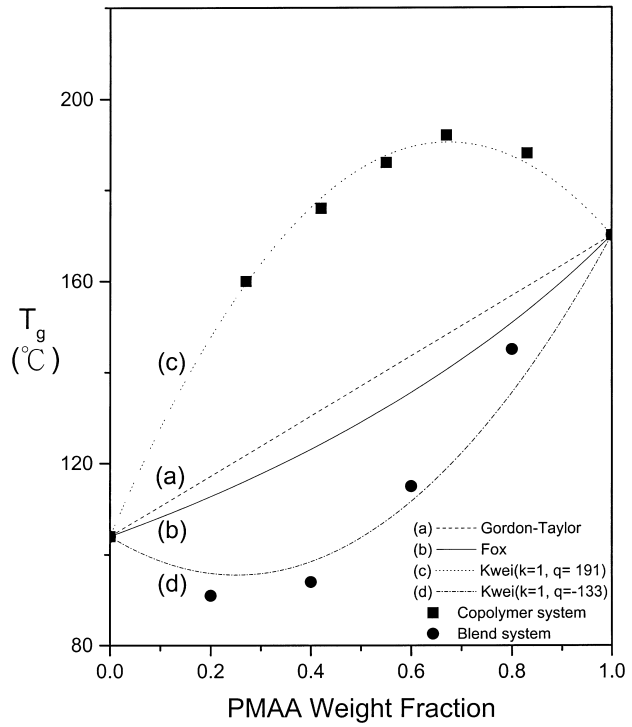

Fig. 4. T_g Vs. composition curves based on (a) the Gordon–Taylor equation (b) the Fox equation (c) the Kwei equation (d) the Kwei equation (●) experimental data of blends (■) experimental data of copolymers.

between polymers [18,19]. Fig. 3 shows the thermograms obtained from 60PMMA to 40PMAA blend, where the first scan shows a single glass transition followed by an endothermic peak centered at 230 °C. After a rapid quench, the consecutive scan behaviors as a two-component system and gives two separate T_g's. The phase separation observed is irreversible and the phase redisolution does not seem to occur for these blends.

Chemical structures of PMMA and PMAA are very similar. Scheme 1 shows IR carbonyl vibrations from the free and hydrogen bonded of PMMA and PMAA. The MAA unit may exit as the free state, self-associated dimmer, or inter-association with PMMA. The IR carbonyl stretching bands of the associated dimmer and free state in MAA unit appear at 1742 and 1699 cm^{-1}, respectively [20]. For the MMA unit, the carbonyl stretching absorptions by free and hydrogen bonded carbonyl groups are at 1730 and 1705 cm^{-1}, respectively [13]. Hence, states of MMA and MAA associations in blends and copolymers can be analyzed by FT-IR spectra. Fig. 5 shows the infrared spectra of the carbonyl stretching measured at room temperature ranging from 1675 to 1770 cm^{-1} for different compositions of PMMA/PMAA blends. By quantitatively measuring the absorptivity ratio of the hydrogen bonded to free bands in a blend system, we can determine the fraction of hydrogen bonded PMMA using the $a_R = a_{HB}/a_F = 1.5$ [21,22]. Through least-squares curve-fitting within the carbonyl stretching region using four Gaussian bands (see Fig. 6(a)–(d)). The first and the second bands are

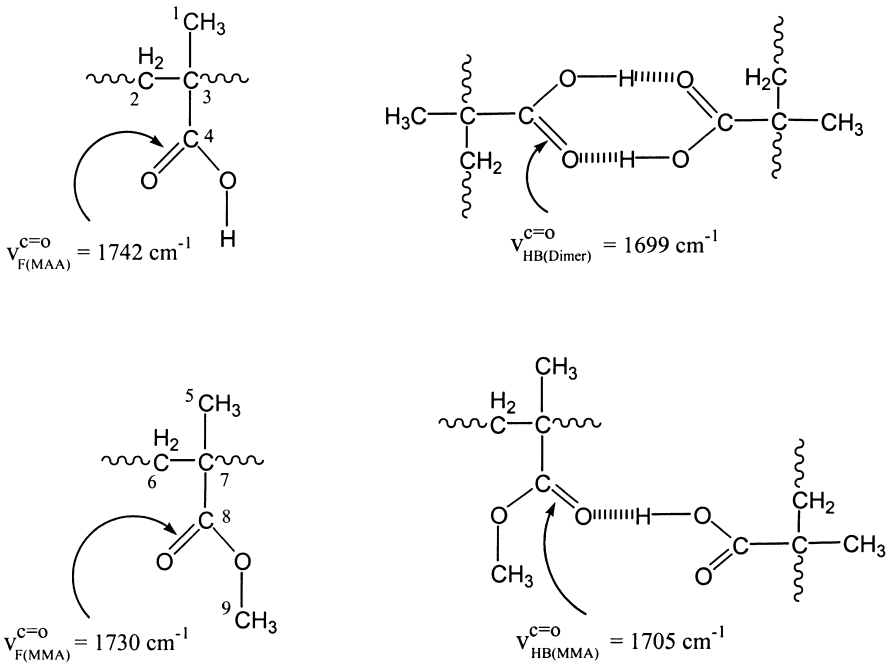

Scheme 1. Schematic diagram showing carbon number and type of interaction between MMA and MAA units.

contributed from free carbonyl (C=O) groups of PMAA and PMMA, respectively. The later two bands are the hydrogen bonded carbonyl groups of PMAA and PMMA, respectively. The parameters of the infrared carbonyl band are summarized in Table 2, where the hydrogen bonded fraction of PMMA increases with the increase in PMAA content.

Fig. 7 shows the conventional second run DSC thermograms of PMMA-*co*-PMAA copolymers with various

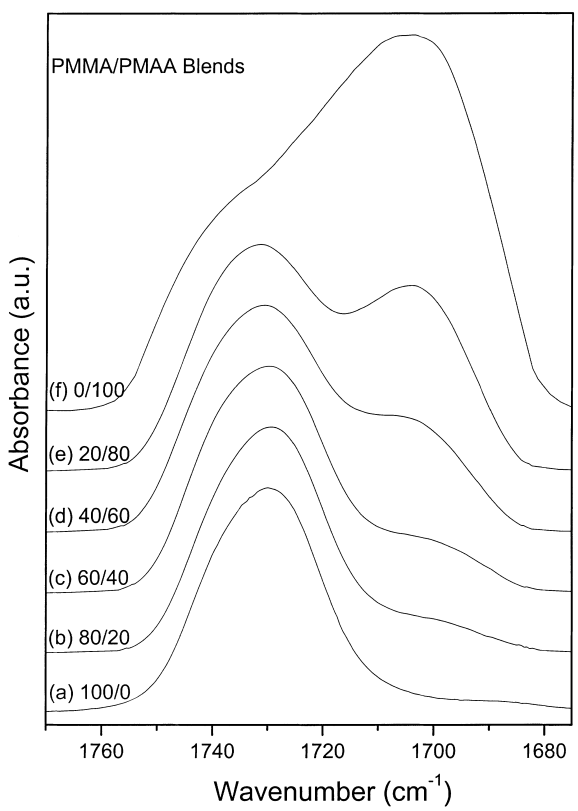

Fig. 5. FT-IR spectra recorded at room temperature in the 1675–1770 cm^{-1} region for various composition of PMMA/PMAA blends.

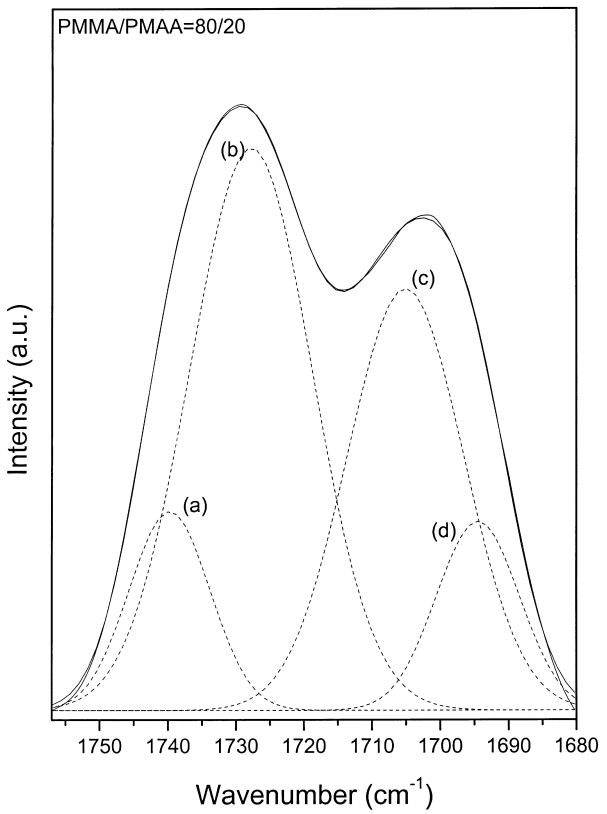

Fig. 6. Example of least-squares curve-fitting results of carbonyl stretching for a PMMA/PMAA = 80/20 blend.

Table 2
PMMA carbonyl group curve-fitting results of the PMMA/PMAA blends and PMMA-*co*-PMAA copolymers

Samples (wt%)	Free C=O				H Bonded C=O				fb[a] (%)
	ν_1	A_{f1}	ν_2	A_{f2}	ν_1	A_{b1}	ν_2	A_{b2}	
80MMA/20MAA	1728	72	1740	15	1704	11	1695	1	9
60MMA/40MAA	1728	65	1740	16	1704	15	1693	2	13
40MMA/60MAA	1727	53	1739	14	1705	27	1694	4	25
20MMA/80MAA	1727	46	1739	10	1705	32	1694	10	32
Pure PMAA	–	–	1741	34	–	–	1700	65	–
73MMA-*co*-27MAA	1730	62	1744	18	1706	17	1693	1	16
58MMA-*co*-42MAA	1730	55	1744	16	1709	24	1695	3	22
45MMA-*co*-55MAA	1731	42	1745	14	1707	33	1694	9	34
33MMA-*co*-67MAA	1731	38	1745	12	1709	34	1695	13	37
17MMA-*co*-83MAA	1731	37	1745	11	1708	38	1694	13	40

ν_1, ν_2 : Wavenumber of PMMA, PMAA (cm^{-1}); A_{f1} : free C=O area fraction of PMMA (%); A_{f2} : free C=O area fraction of PMAA (%); A_{b1} : C=O area fraction of hydrogen bonding of PMMA (%); A_{b2} : C=O area fraction of hydrogen bonding of PMAA (%).
[a] *fb* : PMMA fraction of hydrogen bonding $= (A_{b1}/1.5)/(A_{b1}/1.5 + A_{f1})$.

PMMA–PMAA weight ratios. On the contrary to the previous blend system, the T_g-composition relationship is a positive deviation (Fig. 4(c)) in comparing with that predicted by a liner relationship or the Fox equation. According to the Kwei equation (Eq. (2)), a positive q of 191 is obtained. Fig. 8 shows the infrared spectra of carbonyl stretching measured at room temperature ranging from 1675 to 1800 cm^{-1} for different compositions of PMMA-*co*-PMAA copolymers. Again, the fraction of hydrogen bonded carbonyl absorption also increases with increasing the PMAA component and the curve fitting results are also summarized in Table 2. Fig. 9 plots the fraction of hydrogen bonded carbonyl from PMMA vs. the PMAA weight fraction of the blend and the copolymer systems. The copolymer system, in general, has greater fraction of the hydrogen bonded carbonyl than the corresponding polymer blend due to composition heterogeneities in these hydrogen bonded polymers.

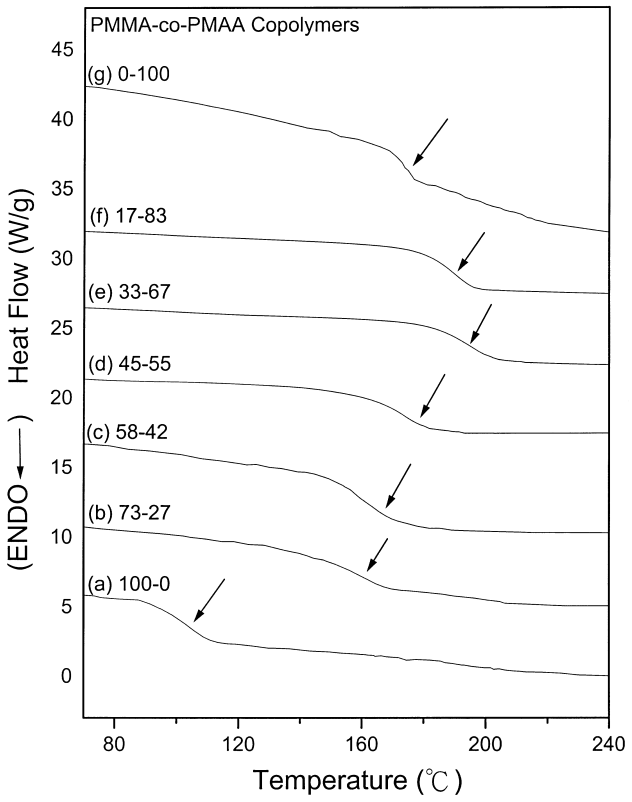

Fig. 7. DSC thermograms of the PMMA-*co*-PMAA copolymers with different compositions (weight ratio): (a) 100–0 (b) 73–27 (c) 58–42 (d) 45–55 (e) 33–67 (f) 17–83 (g) 0–100.

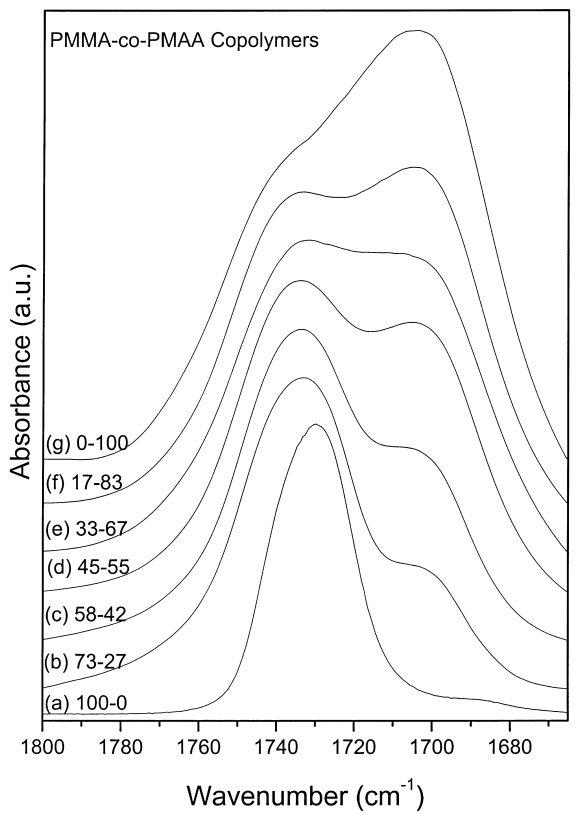

Fig. 8. FT-IR spectra recorded at room temperature in the 1665–1800 cm^{-1} regions for various compositions of PMMA/PMAA blends.

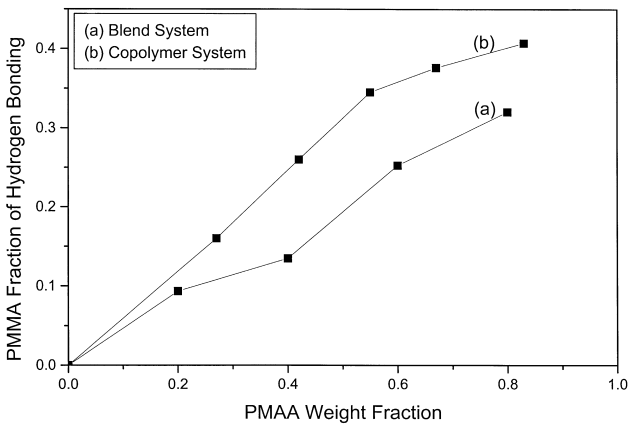

Fig. 9. PMMA fraction of hydrogen bonded carbonyl vs. PMAA content for blends and copolymers.

3.2. Solid-state NMR analyses

Solid-state NMR spectroscopy has been used for better understanding of the phase behavior and morphology of polymer blends and copolymers. Fig. 10 showed the selected ^{13}C CP/MAS spectra of various PMMA/PMAA blends and copolymers. Peak assignments of the ^{13}C CP/MAS spectra of PMMA and PMAA to the structures (see Scheme 1) are indicated in Fig. 10.

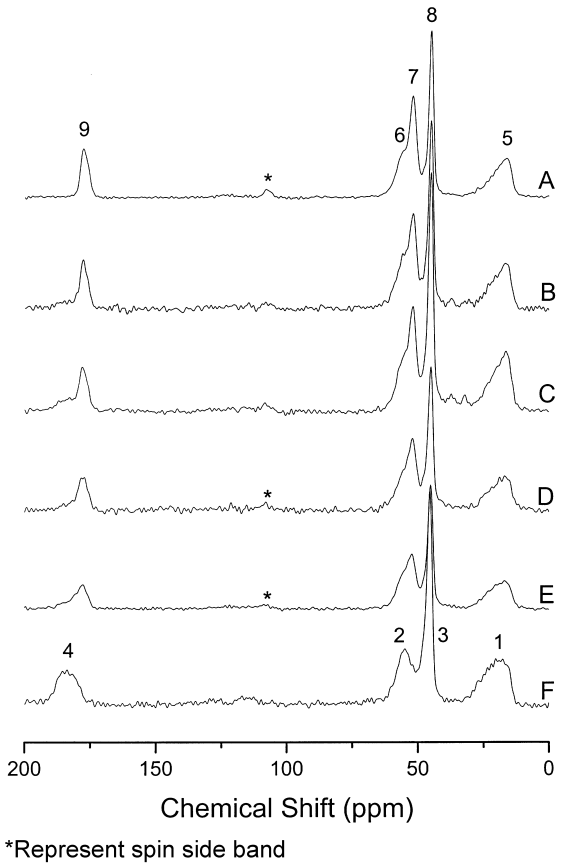

Fig. 10. ^{13}C CP/MAS NMR of PMMA/PMAA blends and copolymers at room temperature: (A) pure PMMA (B) 80PMMA/20PMAA blend (C) 60PMMA/40PMAA blend (D) 73PMMA-*co*-27PMAA copolymer (E) 58PMMA-*co*-42PMAA copolymer.

A single T_g based on DSC analysis implies that the mixing of two blending components in a scale up to about 20–40 nm. The dimension of mixing smaller than 20 nm can be obtained through measurement of the spin-lattice relaxation time in the rotating frame ($T_{1\rho}^H$). The magnetization of resonance is expected to decay according to the following exponential function model by Eq. (3) by the spin-locking mode employed in this study.

$$\ln(M_\tau/M_0) = -\tau/T_{1\rho}^H \tag{3}$$

where $T_{1\rho}^H$ is the spin-lattice relaxation time in the rotating frame, τ is the delay time used in the experiment, and M_τ is the corresponding resonance. $T_{1\rho}^H$ can be obtained from the slope of $\ln(M_\tau/M_0)$ vs. τ. Fig. 11 shows the plots of $\ln(M_\tau/M_0)$ vs. τ for the main chain non-protonated aliphatic carbon and the methylene to realize the homogeneity of the polymer chain. Data from Figs. 11 and 12 are both in good agreement with Eq. (3). From the slope of the fitting line, the $T_{1\rho}^H$ value can be determined.

A single composition-dependent $T_{1\rho}^H$ is obtained for all PMMA/PMAA blends and PMMA-*co*-PMAA copolymers, suggesting that both blends and copolymers are homogeneous to a scale where the spin-diffusion occurs within the time $T_{1\rho}^H$. The upper spatial scale of the spin-diffusion path length L can be estimated from the following expression [23–25]:

$$L = (6DT_{1\rho}^H)^{1/2} \tag{4}$$

where D, which is typically assumed to be 10^{-16} m^2 s^{-1}, an effective spin-diffusion coefficient depending on the average proton to proton distance as well as the dipolar interaction. Hence, the upper spatial scales of the domain sizes are estimated to be around 2 nm for the PMMA/PMAA blends and copolymers. Fig. 13 plots the $T_{1\rho}^H$ values of PMMA/PMAA blends and PMMA-*co*-PMAA copolymers. The

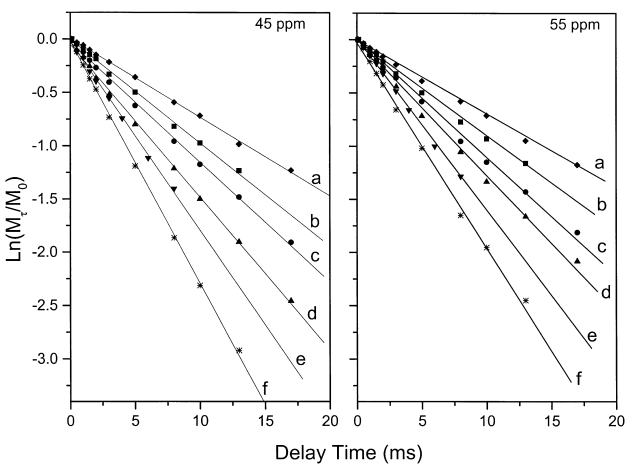

Fig. 11. Semi-logarithmic plots of the magnetization intensities of 45 and 55 ppm vs. delay time for PMMA/PMAA blends with a contact time of 1.0 ms: (a) 100/0 (b) 80/20 (c) 60/40 (d) 40/60 (e) 20/80 (f) 0/100.

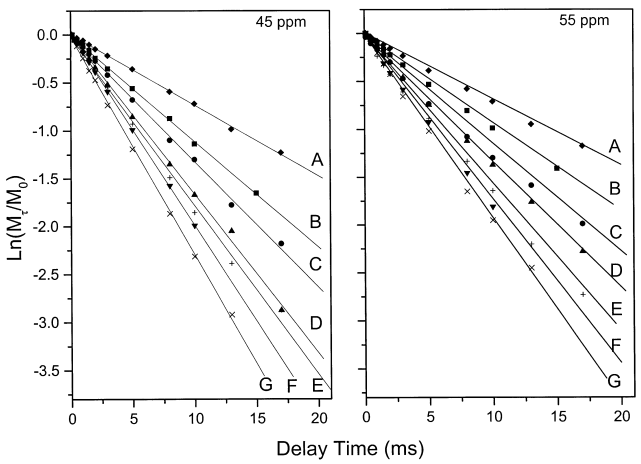

Fig. 12. Semi-logarithmic plots of the magnetization intensities of 45 and 55 ppm vs. delay time for PMMA-*co*-PMAA copolymers with a contact time of 1.0 ms: (A) 100–0 (B) 73–27 (C) 58–42 (D) 45–55 (E) 33–67 (F) 17–83 (G) 0–100.

average relaxation time can be predicted by a general model for pure components [26–28]

$$\frac{1}{T_{ji}} = \left(\frac{N_A M_A}{N_T}\right)\left(\frac{1}{T_{Ai}}\right) + \left(\frac{N_B M_B}{N_T}\right)\left(\frac{1}{T_{Bi}}\right) \tag{5}$$

where $1/T_{Ai}$ and $1/T_{Bi}$ are the relaxation times of pure components A and B, respectively. N_A and N_B are the numbers of protons per mole of the respective components. M_A and M_B are the mole fractions of the component, and $N_T = N_A M_A + N_B M_B$. As shown in Fig. 13, it can be seen that for each blend, the relaxation times derivates from the composition average line. $T_{1\rho}^H$ of copolymers have greater agreement with the prediction line than blends, indicating that the degrees of homogeneity of copolymers are relatively higher than those of blends.

3.3. Kovacs' free volume theory analyses

In order to simplify the qualitative analysis on free volume change in these blend and copolymer systems, the Kovacs' free volume theory [29,30] is adopted. The hypothesis of the Kovacs' free volume theory is that the fractional free volume of the mixture f is given by the weighed sum of the fractioned free volumes of pure components f_i plus an interaction term:

$$f = \Phi_1 f_1 + \Phi_2 f_2 - g\Phi_1\Phi_2 \tag{6}$$

where Φ_i is the volume fraction of the components i and the term, $g\Phi_1\Phi_2$, represents the fraction of excess volume in the mixture:

$$g\Phi_1\Phi_2 = V_e/V \tag{7}$$

V is the total volume of the blend, V_e is the excess volume (Eq. (1)). According to Kovacs' free volume theory [29], if the T_g difference ($T_{g1} - T_{g2}$) between component 1 and 2 is larger than 50 °C, the free volume of the higher T_g polymer becomes zero at a critical temperature T_c, and the corresponding critical volume fraction (Φ_c) calculated by Kovacs is:

$$T_c = T_{g1} - \frac{f_{g1}}{\Delta\alpha_1} \tag{8}$$

$$\Phi_c = f_{g1}\left[\Delta\alpha_2(T_{g1} - T_{g2}) + f_{g1}\left(1 - \frac{\Delta\alpha_1}{\Delta\alpha_2}\right)\right] \tag{9}$$

The composition dependence of T_g above T_c is given by:

$$T_g = \frac{\Phi_2 T_{g2} + K\Phi_1 T_{g1} + (g/\Delta\alpha_2)\Phi_2\Phi_1}{\Phi_2 + K\Phi_1} \tag{10}$$

where $K = \Delta\alpha_1/\Delta\alpha_2$ and $\Delta\alpha_i$ the difference between the volume expansion coefficient in the liquid and glassy states of the i component.Below T_c, T_g is given by

$$\frac{T_g - T_{g2}}{\Phi_1} = \frac{g}{\Delta\alpha_2} + \left(\frac{f_{g1}}{\Delta\alpha_2}\right)\frac{1}{\Phi_2} \tag{11}$$

Therefore, the $f_{g1}/\Delta\alpha_2$ can be calculated by a plot of $(T_g - T_{g2})/\Phi_1$ vs. $1/\Phi_2$ from its slope and the $g/\Delta\alpha_2$ from its intercept. In our study, the experimental data of blend

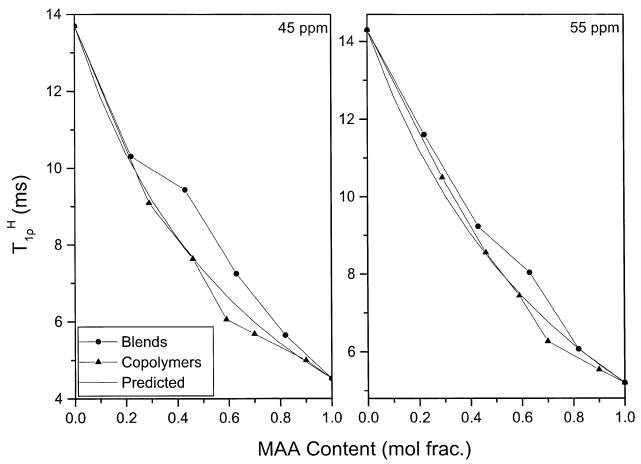

Fig. 13. Comparison of $T_{1\rho}^H$ values for the PMMA/PMAA blends and copolymers.

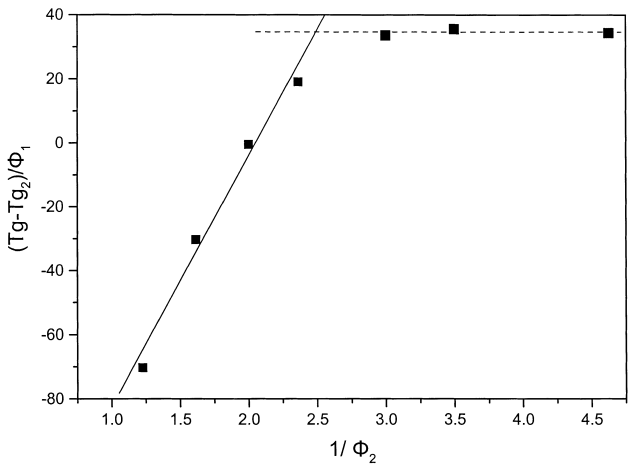

Fig. 14. Analysis of the experimental data for PMMA/PMAA blends based on Kovacs' free volume theory.

system with T_g both below T_c can be used by this theory using Eq. (11) as shown in Fig. 14. Both $\Delta\alpha_2$ and g can be obtained by taking the classical value of 0.025 for f_{g1} [31,32]. $\Delta\alpha_2$ and g are obtained as 3.2×10^{-4} and -0.017, respectively. A negative value of the Kovacs' g parameter reflects an increase in the free volume in the polymer mixture. In copolymer system with T_g both above T_c, we can use Eq. (10) to obtain the $g = 0.02$, implying that a decrease of the free volume in these copolymers. Comparisons on experimental and predicted excess volumes are shown in Fig. 15. These experimental values are agreed well with prediction.

A negative value of the Kovacs' g parameter has been obtained for blend system, therefore, an increase of the free volume is expected from the negative deviation of T_g analysis. Again, a positive value of the Kovacs' parameter g for copolymer is coincided with the positive deviation of T_g analysis. The above results can be rationalized in terms of stronger hydrogen bonding interactions for copolymer system in FT-IR analysis.

4. Conclusions

Both PMMA-*co*-PMAA copolymers and PMMA/PMAA blends were investigated by using FT-IR, DSC, and high-resolution solid-state ^{13}C NMR. All the blends are totally miscible in the amorphous phase over entire compositions. The T_g of the PMMA-*co*-PMAA is significantly higher than that from the liner relationship or the Fox equation. On the contrary, the T_g of the PMMA/PMAA blend is lower than the average value. Measurements of $T_{1\rho}^H$ reveal that all blends and copolymers possess single composition-dependent, indicating a good miscibility and chain dynamic on a scale of 1–2 nm. However, the $T_{1\rho}^H$ of the copolymer is smaller than the corresponding blend, implying that the degree of homogeneity of the copolymer is still higher than that of the blend due to higher miscibility of the copolymer. On the basis of Kovacs' free volume theory, the free volume of the copolymers is significantly less than the average value, another indication of greater homogeneity of the copolymer than the corresponding blend. Better homogeneity of the copolymer than the blend can also be rationalized in terms of extent of hydrogen bonding interaction, the fraction of the hydrogen bonded carbonyl from PMMA of copolymer is stronger than the blend base on FT-IR analyses.

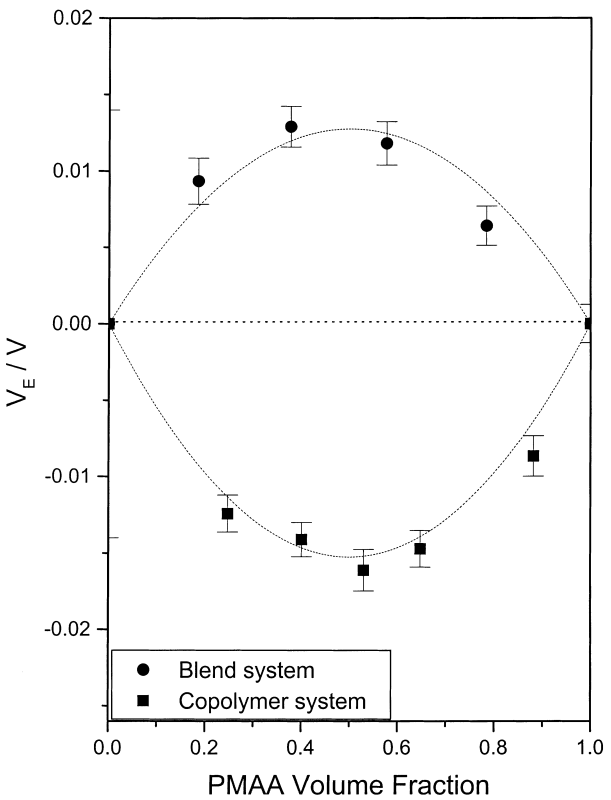

Fig. 15. Excess volume of mixing for (●) PMMA/PMAA blends (■) PMMA-*co*-PMAA copolymers and (—) predicted by Kovacs' free volume theory.

Acknowledgements

This research was financially supported by the National Science Council, Taiwan, Republic of China, under Contract Nos. NSC-91-2216-E-009-018.

References

[1] Chu PP, Huang MH, Huang WJ, Chang FC. Macromolecules 2000; 33:9630.
[2] Huang WJ, Chang FC, Chu PP. Polymer 2000;41:6051.
[3] Huang WJ, Chang FC, Chu PP. Polymer 2000;41:6095.
[4] Kuo SW, Chang FC. Macromolecules 2001;34:7737.
[5] Coleman MM, Xu Y, Painter PC. Macromolecules 1994;27:127.
[6] Coleman MM, Graf JF, Painter PC. Specific interactions and the miscibility of polymer blends. Lancaster: Technomic Publishing; 1991.
[7] Kennedy JP, Kelen T, Tudos F. J Polym Sci, Polym Chem Ed 1975; 13:2277.
[8] Kuo SW, Chang FC. Polymer 2001;42:9843.
[9] Harwood HJ, Ritchey WM. J Polym Sci: Part B, Polym Phys 1964;2: 601.
[10] Roman SJ, Madruga EL, del Puerto MA. J Polym Sci, Polym Chem Ed 1983;21:3303.
[11] Fox TG. Bull Am Phys Soc 1956;2:123.
[12] Kwei TK. J Polym Lett Ed 1984;22:307.
[13] Kuo SW, Chang FC. Macromolecules 2001;34:4089.
[14] Iriarte M, Alberdi M, Shenoy SL, Iruin JJ. Macromolecules 1999;32: 2661.
[15] Chen X, An L, Li L, Yin J, Sun Z. Macromolecules 1999;32:5905.
[16] Uriarte C, Eguiazabal JI, Llanos M, Iribarren JI, Iriun JJ. Macromolecules 1987;20:3038.
[17] Natansohn A. J Polym Sci, Polym Lett Ed 1985;23:305.
[18] Shen S, Torkelson JM. Macromolecules 1992;25:721.
[19] Cesteros LC, Isasi JR, Katime I. Macromolecules 1994;27:7887.
[20] Motzer HR, Painter PC, Coleman MM. Macromolecules 2001;34: 8390.

[21] Cortazar M, Pomposo JA. Macromolecules 1994;27:252.
[22] Serman CJ, Painter PC, Coleman MM. Polymer 1991;32:1049.
[23] McBrierty VJ, Douglass DC. J Polym Sci Macromol Rev 1981;16: 295.
[24] Demco DE, Johansson A, Tegenfeldt J. Solid State Nucl Magn Reson 1995;4:13.
[25] Clauss J, Schmidt-Rohr KWH. Acta Polym 1993;44:1.
[26] Kovacs AJ. Adv Polym Sci 1963;3:394.
[27] Braun G, Kovacs AJ. Physics of non-crystalline solids. Amsterdam: North-Holland; 1965.
[28] Dickson LC, Yang H, Chu CW, Stein RS, Chien JCW. Macromolecules 1987;20:1757.
[29] McBriety VJ, Douglass DC, Kwei TW. Macromolecules 1978;11:1265.
[30] Asana A, Takegoshi K, Hikichi K. Polymer 1994;35:5630.
[31] Williams ML, Landel RF, Ferry JD. J Am Chem Soc 1955;77:3701.
[32] Ferry JD. Viscoelastic properties of polymers. New York: Wiley; 1980.